

1 Experimental test of the cooling rate effect on blocking 2 temperatures in stepwise thermal demagnetisation

3 Thomas A. Berndt^{1*}, Liao Chang², Greig A. Paterson^{3,4}, Changqian Cao^{4,5}

4 *¹ Department of Geophysics, School of Earth and Space Sciences,*

Peking University, Beijing 100871, P. R. China

5 *² Laboratory of Orogenic Belts and Crustal Evolution, School of Earth and Space Sciences,*

Peking University, Beijing 100871, P. R. China

6 *³ Department of Earth, Ocean and Ecological Sciences, University of Liverpool,*

Liverpool, L69 7ZE, UK

7 *⁴ Key Laboratory of Earth and Planetary Physics, Institute of Geology and Geophysics,*

Chinese Academy of Sciences, Beijing 100029, China

8 *⁵ France-China Bio-Mineralization and Nano-Structures Laboratory,*

Chinese Academy of Sciences, Beijing, China

9

10 SUMMARY

11 Upon cooling, most rocks acquire a thermoremanent magnetisation (TRM); the cool-
12 ing rate at which this happens not only affects palaeointensity estimates, but also their
13 unblocking temperatures in stepwise thermal demagnetisation experiments, which is im-
14 portant, for example, to estimate volcanic emplacement temperatures. Traditional single-
domain (SD) theory of magnetic remanence relates relaxation times to blocking tem-
peratures – the blocking temperature is the temperature at which the relaxation time
becomes shorter than the experimental timescale – and therefore strictly only applies
to remanence acquisition mechanisms at constant temperatures (i.e., viscous remanent
magnetisations, VRMs). A theoretical framework to relate (constant) blocking tempera-

tures to (time-varying) cooling rates exists, but this theory has very limited experimental verification – partly due to the difficulty of accurately knowing the cooling rates of geological materials. Here we present an experimental test of this “cooling rate effect on blocking temperatures” through a series of demagnetisation experiments of laboratory-induced TRMs with controlled cooling rates. The tested cooling rates span about 1 order of magnitude and are made possible through (1) extremely accurate demagnetisation experiments using a low-temperature magnetic properties measurement system (MPMS), and (2) the employment of a “1-step-only” stepwise thermal demagnetisation protocol where the relaxation process is measured over time. In this way the relaxation time corresponding to the blocking temperature is measured, which can be done to much higher accuracy than measuring the blocking temperature directly as done in traditional stepwise thermal demagnetisation experiments. Our experiments confirm that the cooling rate relationship holds to high accuracy for ideal magnetic recorders, as shown for a synthetic weakly interacting SD magnetoferitin sample. A SD-dominated low-Ti titanomagnetite Tiva Canyon Tuff sample, however, showed that natural samples are unlikely to be sufficiently “ideal” to meet the theoretical predictions to high accuracy – the experimental data agrees only approximately with the theoretical predictions, which may potentially affect blocking temperature estimates in stepwise thermal demagnetisation experiments. Moreover, we find a strongly enhanced cooling rate effect on palaeointensities for even marginally non-ideal samples (up to 43 % increase in pTRM for a halving of the cooling rate).

Key words: Magnetic mineralogy and petrology; Palaeointensity; Palaeomagnetism; Remagnetization; Rock and mineral magnetism.

38 1 INTRODUCTION

39 Most igneous rocks contain ferromagnetic minerals that, upon cooling, acquire a thermoremanent
40 magnetisation (TRM, see Appendix for a list of acronyms) aligned with the Earth’s ambient magnetic

* Email: thomasberndt@pku.edu.cn

41 field. Subsequently, these rocks may acquire overprints of partial TRMs (pTRM) due to re-heating, or
 42 of viscous remanent magnetisations (VRM) due to exposure to magnetic fields over very long times.
 43 The temperatures at which VRMs/TRMs are acquired (blocking temperature) T_A play an important
 44 role, for example, to determine emplacement temperatures (McClelland & Druitt, 1989; Paterson et al.,
 45 2010b) and for viscous remanent magnetisations (VRM) dating (Heller & Markert, 1973; Berndt &
 46 Muxworthy, 2017; Sato et al., 2014). The different natural remanent magnetisation (NRM) compo-
 47 nents can be isolated in thermal demagnetisation experiments, during which the sample is heated
 48 to successively higher temperatures in zero-field to progressively demagnetise the sample and deter-
 49 mine the demagnetisation (unblocking) temperature T_D , at which a NRM component is completely
 50 removed. The blocking temperature is defined to be the temperature at which the experimental or geo-
 51 logical timescale of the (de)magnetisation process is longer than the relaxation time of the particles –
 52 for SD particles, the two can be related to each other using contour plots of relaxation time vs. block-
 53 ing temperature called nomograms (Néel, 1949; Pullaiah et al., 1975). Nomograms are widely used
 54 to relate blocking temperatures measured in the laboratory to blocking temperatures of remanence ac-
 55 quisition due to geological processes: one first finds the “laboratory point” described by the measured
 56 (un)blocking temperature and the laboratory timescale (typically minutes) and than extends along the
 57 corresponding contour to either the geological timescale or the geological temperature of the rema-
 58 nence acquisition process in question (whichever is known) in order to infer the other. Experimental
 59 tests of this relationship are generally positive (Dunlop & Özdemir, 1993; Dunlop et al., 2000; Jack-
 60 son & Worm, 2001), though sometimes anomalously high demagnetisation temperatures have been
 61 observed (Dunlop, 1983; Kent, 1985; Kent & Miller, 1987); these are often attributed to pseudo-SD
 62 (PSD)/vortex and multidomain (MD) grains (Dunlop et al., 2000).

63 Strictly speaking, however, TRM acquisition is a process at non-constant temperature: it occurs
 64 during cooling. The cooling rate is known to have a notable effect on palaeointensities, but they also
 65 affect unblocking temperatures: The faster a rock is cooled, the lower the apparent blocking temper-
 66 ature (since faster cooling is equivalent to a shorter relaxation time) – the effect is therefore critical
 67 for estimation of emplacement/re-heating temperatures. York (1978a,b) and Dodson & McClelland-
 68 Brown (1980) derived relationships to correct blocking temperatures for the cooling rate r_A . These
 69 equations are, however, difficult to test experimentally, since this would require precisely known geo-
 70 logical cooling rates, as well as very high-resolution stepwise thermal demagnetisation (STD) exper-
 71 iments. Various authors studied the effect of the cooling rate on palaeointensities and the necessary
 72 cooling rate corrections (Halgedahl et al., 1980; Fox & Aitken, 1980; Brown, 1963; Ferk et al., 2010;
 73 Muxworthy & Heslop, 2011; Muxworthy et al., 2011; Biggin et al., 2013; Muxworthy et al., 2013;
 74 Santos & Tauxe, 2019), but few have focused on blocking temperatures.

We recently published a study where, through very accurate continuous thermal demagnetisation (CTD) experiments of laboratory induced TRMs and VRMs in a Magnetic Properties Measurement System (MPMS), we were able to experimentally test the heating rate effect on blocking temperatures (Berndt et al., 2017). The heating rate is the converse of the cooling rate effect: during CTD, a sample is heated at a heating rate r_D – the faster this rate, the higher the demagnetisation temperature T_D . Through these experiments we found slight deviations from the theoretically predicted blocking temperatures, both for experiments involving (1) only the heating rate effect (i.e. CTD of VRMs), and (2) both the heating and the cooling rate effect (i.e. CTD of TRMs), which we suggested to correct empirically for. Here, we present a second set of experiments on the same samples, where we used a modification of the experimental setup to allow for the study of the cooling rate effect in isolation: We experimentally tested (1) the cooling rate effect representative of STD of a TRM, as is important e.g. for the estimation of volcanic emplacement temperatures (e.g. Paterson et al., 2010b), and (2) the relaxation-time–blocking-temperature relationship from the well-known Pullaiah nomograms / Néel theory, as is important e.g. for VRM dating studies employing STD (e.g. Sato et al., 2014). While Berndt et al. (2017) studied CTD experiments (relevant, for example, for VRM dating employing CTD (e.g. Berndt & Muxworthy, 2017)), here we experimentally test the more common STD experiments.

91 2 THEORETICAL PREDICTIONS

The relaxation time of a rock containing non-interacting SD particles is given by Néel (1949),

$$\frac{1}{\tau} = \frac{2}{\tau_0} \exp \left\{ -\frac{\mu_0 M_s H_K V}{kT} \right\}, \quad (1)$$

where τ_0 is the atomic attempt time, μ_0 is the vacuum permeability, M_s is the spontaneous magnetisation, H_K is the microscopic coercivity, V is the grain volume, k is the Boltzmann constant and T is temperature. Magnetic blocking occurs when the temperature falls below the point where the relaxation time τ becomes large (relative to the time of either the experiment or of the natural magnetisation process). The factor 2 in eq. (1) accounts for blocking in zero external fields (i.e. demagnetisation) – for remanence acquisition in a (weak) magnetic field (i.e. acquisition), the factor 2 must be omitted. In this paper we denote the relaxation time in field (acquisition) by t_A , and in zero field (demagnetisation) by t_D . Similarly, acquisition and demagnetisation temperatures are denoted by T_A and T_D , respectively. Eq. (1) allows us to relate acquisition and demagnetisation times and temperatures (Pullaiah et al., 1975):

$$\frac{T_A \ln(t_A/\tau_0)}{1 - (T_A/T_C)} = \frac{T_D \ln(2t_D/\tau_0)}{1 - (T_D/T_C)}, \quad (2)$$

where T_C is the Curie temperature. In this relation, the temperature variation of M_s and H_K is assumed to be proportional to $\sqrt{1 - T/T_C}$, as applicable for (titano)magnetite (e.g. Aharoni, 2000). This relationship is well-established for SD grains and has often been confirmed experimentally, but since it assumes constant temperatures, it only applies to VRMs. TRMs, however, are acquired upon cooling at a rate r_A . York (1978a,b), as well as Dodson (1976) and Dodson & McClelland-Brown (1980), derived an expression to relate T_A and r_A to the demagnetisation temperature and time T_D and t_D . Berndt et al. (2017) introduced the notation of the *effective* relaxation time t_{eff} , which is approximately given by

$$t_{eff} = \frac{T_A}{r_A} \left(1 - \frac{T_A}{T_C} \right) / \ln \left(\frac{2T_A}{r_A \tau_0} \left(1 - \frac{T_A}{T_C} \right) \right). \quad (3)$$

The effective relaxation time can be inserted in place of t_A into eq. (2) to obtain demagnetisation times and temperatures of (p)TRMs – it hence plays the role of “converting” cooling rates r_A to equivalent acquisition times t_A that would create an equivalent remanence at a constant temperature. Both eq. (2) and eq. (3) are tested experimentally in this study.

3 SAMPLES

Two of the same samples used by Berndt et al. (2017) were re-used in this study: The Tiva Canyon Tuff sample TC04-12-01K (provided by the Institute for Rock Magnetism, University of Minnesota) and the magnetoferitin sample MFn1 (produced at the Institute of Geology and Geophysics, Chinese Academy of Sciences). The Tiva Canyon sample contains fine-grained low-Ti titanomagnetite, which is mostly super-paramagnetic (SP) at room temperature (Till et al., 2011). The titanium content is ca. 10 % (TM10) (Jackson et al., 2006) and grains are highly elongated needles around 15 nm in length (Schlanger et al., 1991; Berndt et al., 2015). Its Curie temperature was previously determined from thermomagnetic $M_s(T)$ curves to be 471°C (Berndt et al., 2015), which implies a slightly higher Ti-content in this particular sample of ca. TM20. The Verwey transition (Verwey, 1939) is suppressed in the samples due to the Ti impurities (Worm & Jackson, 1999). First-order reversal-curves (FORC) indicated negligible magnetostatic interactions (Berndt et al., 2015).

The magnetoferitin is synthesised through biomimetic mineralisation inspired by biological processes in nature, and contains rounded stoichiometric magnetite particles of ca. 8 nm diameter, surrounded by a protein shell prevents clustering of particles and reduces magnetostatic interactions (Cao et al., 2010, 2014), however, Transmission electron microscopy showed some degree of clustering. It also showed that 90 % of the particles are between 6.2 and 11.6 nm diameter and aspect ratios between 1.01 and 1.38 (Berndt et al., 2017). The sample is completely SP above 150 K, but stable uniaxial SD

6 Berndt et al.

114 at low temperatures – with a saturating field of 200 mT at 10 K (Berndt et al., 2017). It was stored
115 sealed and refrigerated since their use by Berndt et al. (2017).

116 4 METHOD

117 4.1 Viscous demagnetisation protocol

118 Eq. (2) and eq. (3) are experimentally validated in this work: the first provides another confirmation
119 of Pullaiah nomograms for SD grains to relate blocking temperatures in STD experiments to VRMs,
120 and the second to determine cooling rates and hence to enable the use of Pullaiah style diagrams for
121 estimation of emplacement temperatures of (p)TRMs. The experiments presented here closely follow
122 the procedure of Berndt et al. (2017), with a specific modification to test the cooling rate effect in
123 isolation – the use of a viscous demagnetisation protocol. We first outline the VRM experiments:

124 (i) First, a (demagnetised) sample is cooled in zero field in an MPMS to a set temperature T_A (33
125 to 38 K for the magnetoferitin, 53 to 58 K for the Tiva Canyon) and a VRM is imparted in a field H_0
126 of 50 μ T for a set time t_A (between 750 s and 12,000 s).

127 (ii) The field is switched off, and the sample is quickly heated or cooled to a target demagnetisation
128 temperature T_D (35 K for the magnetoferitin, 55 K for Tiva Canyon).

129 (iii) The viscous decay of the magnetisation is measured in zero field for up to 12,000 s (Fig. 1a) –
130 the “1-step-only” thermal demagnetisation.

131 (iv) The sample is heated up to room temperature and cooled again in zero field to remove any
132 possible remaining remanence.

133 (v) The process is then repeated at various different acquisition times and temperatures.

134 From this protocol, T_A , t_A , and T_D are known parameters. Hence, to test the validity of eq. (2), t_D
135 must be determined from the viscous demagnetisation experiment and compared against the theoretical
136 predictions.

137 In order to test eq. (3) (to estimate blocking temperatures of pTRMs such as volcanic emplace-
138 ment temperatures), the first step in the procedure above is modified: First, a (demagnetised) sample is
139 cooled in zero field in an MPMS at a fixed cooling rate r_A (between 0.04 and 0.32 K/min) to the target
140 demagnetisation temperature T_D (35 K for the magnetoferitin, 55 K for Tiva Canyon). At the instant
141 the temperature dropped below the predefined acquisition temperature T_A , the 50 μ T field was applied
142 to impart a pTRM. The cooling process was continued without interruption till the target demagneti-
143 sation temperature T_D was reached, at which point the field was switched off, the temperature was
144 kept constant and the viscous decay of the sample was measured as outlined above. For pTRMs, t_A is

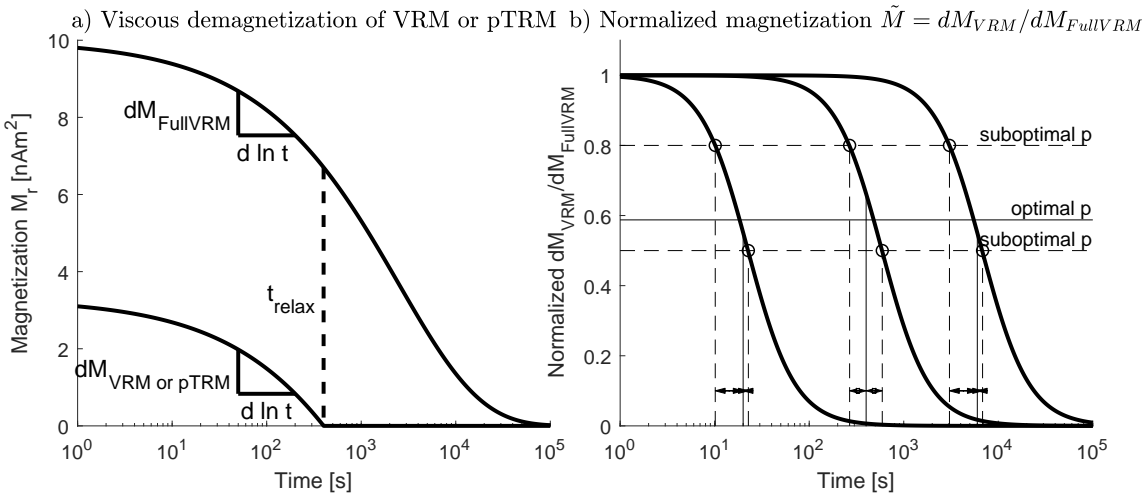


Figure 1. a) Schematic drawing of the viscous demagnetisation protocol. The remanent magnetisation curves during viscous demagnetisation of a “full VRM” and partial TRMs/VRMs are shown. “Full VRM” refers to a VRM of high acquisition temperature and very long acquisition time, such that there is still a significant remanence left at the end of the demagnetisation experiment; Partial TRMs/VRMs demagnetise completely during the demagnetisation experiment (in this example a 400 s VRM). Note that the shape of the curves depends on the grain size distribution, but are identical before the relaxation time t_D is passed. b) Schematic drawing of the normalised magnetisation \tilde{M} curves (bold lines) for three VRMs with expected demagnetisation times of 20 s, 400 s (corresponding to the one in (a)) and 6000 s (solid lines). The parameter p is the percentage of normalised magnetisation decay that is used to define the demagnetisation time t_D . Dashed lines show different choices of p (arbitrary values for illustrative purposes). For any possible choice of p , there will be some degree of mismatch (arrows) between the expected demagnetisation times (solid lines) and measured demagnetisation times (dashed lines); p is chosen to minimise the mismatches.

145 the effective time t_{eff} of acquisition and is calculated from r_A using eq. (3) and compared against the
146 prediction from eq. (2) using the known T_A , t_A , and T_D to test the validity of eq. (3).

147 The procedure is analogous to classical experimental tests of nomograms that use STD of known
148 VRMs or pTRMs (Dunlop & Özdemir, 1993): in these, the sample is subjected to progressively higher
149 temperatures to demagnetise the VRM/pTRM. At each heating step, the temperature is held constant
150 for a certain amount of time, such that t_D is fixed and known, and the temperature T_D at which
151 the sample is demagnetised, is to be determined from the experiment. The viscous demagnetisation
152 protocol effectively uses only one fixed and known temperature step T_D – effectively being a “one-
153 step-only” STD protocol. By continuously measuring the magnetisation, it is possible to determine the
154 relaxation time t_D corresponding to this particular heating step.

155 Note that in order to achieve a 50 μT field in the MPMS, the copper coils of the MPMS were used
156 to apply a field (the superconducting coils were left off during the whole experiment). The copper

¹⁵⁷ coils were carefully calibrated to offset any residual field during the demagnetisation experiment and
¹⁵⁸ to yield a total 50 μT field during the acquisition experiment.

¹⁵⁹ **4.2 Removing grain size dependence**

¹⁶⁰ In STD experiments, the demagnetisation temperature is defined as the temperature where the rema-
¹⁶¹ nent magnetisation $M_r(T)$ drops to zero. In viscous demagnetisation, T_D is held constant and $M_r(t)$
¹⁶² continuously decreases. The exact shape of the $M_r(t)$ curve depends on the grain size and coercivity
¹⁶³ distributions of the sample. Moreover $M_r(t)$ approaches zero only asymptotically. Hence, an exact
¹⁶⁴ definition is needed to determine t_D . Based on the approach by Berndt et al. (2017), the procedure is
¹⁶⁵ illustrated in Fig. 1: First, we consider the most stable VRM of our set of experiments and call it a “full
¹⁶⁶ VRM”. Acquired at a temperature $T_{A,full}$ (37 K for the magnetoferitin, 57 K for Tiva Canyon) for a
¹⁶⁷ long time $t_{A,full}$ (6000 s for the magnetoferitin, 12,000 s for Tiva Canyon), this VRM is sufficiently
¹⁶⁸ stable that it did not completely demagnetise over the course of the viscous demagnetisation over the
¹⁶⁹ following 12,000 s. Therefore, the demagnetisation curve $M_{FullVRM}$ only approaches zero asymp-
¹⁷⁰ totically, as schematically indicated in Fig. 1a. The procedure is analogous to that used by Berndt
¹⁷¹ et al. (2017), in which the samples were demagnetised thermally (i.e. continuous heating), rather than
¹⁷² viscously, such that Fig. 1 would show temperature rather than time on the x-axis.

Next, the VRM and pTRM experiments described above are carried out, yielding various viscous demagnetisation curves, $M_{VRM}(t)$ or $M_{pTRM}(t)$, respectively, each of which with T_A and/or t_A smaller than T_D and/or t_D , respectively. Consequently, the VRMs/pTRMs do completely demagnetise over the course of the experiment, as indicated in Fig. 1a. Before the VRM/pTRM is completely demagnetised, the shape of $M_{VRM}(t)$ or $M_{pTRM}(t)$ is still dependent of the grain size/coercivity distribution, but is the same as $M_{FullVRM}(T)$, since the exact same grains are being demagnetised. After the VRM/pTRM is completely demagnetised, $M_{VRM}(t)$ or $M_{pTRM}(t)$ should obviously equal zero. Therefore, one can define the “normalised magnetisation” \hat{M} as the ratio between the derivative of the VRM or pTRM demagnetisation curves and the derivative of the full VRM, i.e.

$$\hat{M} = \frac{dM_{VRM \text{ or } pTRM}/d\ln t}{dM_{FullVRM}/d\ln t}, \quad (4)$$

which should be close to one for $t < t_D$ and close to zero for $t > t_D$ (Fig. 1b). More mathematically, if the grain size distribution is given by $f(V)$, and $n(V)$ is the net proportion of grains of volume V that are magnetised along the field direction,

$$M_{FullVRM} = \int M_s V f(V) n_{FullVRM}(V) dV, \quad (5)$$

and

$$M_{pTRM \text{ or } VRM} = \int M_s V f(V) n_{pTRM \text{ or } VRM}(V) dV, \quad (6)$$

and therefore

$$\hat{M} = \frac{dM_{pTRM \text{ or } VRM}}{dM_{FullVRM}} = \frac{n_{pTRM \text{ or } VRM}}{n_{FullVRM}}. \quad (7)$$

173 Note that, while each of the magnetisations (VRM, pTRM, full VRM) depends on the grain size
 174 distribution, the normalised magnetisation \hat{M} does not depend on the grain size distribution.

175 4.3 Determination of the relaxation time t_D

176 Before taking the derivatives of the $M(t)$ curves, the data was smoothed through a best-fit logistic
 177 function. While \hat{M} should theoretically be a step-function, in practice the curve is smoothed out, due
 178 to the statistical nature of (un)blocking (Fig. 1b). To determine the relaxation times t_D from these,
 179 one has to choose a point where \hat{M} decayed to a proportion p of its initial value; p is chosen as a
 180 best-fit parameter that minimises the mismatch between the “measured relaxation times t_D ” and the
 181 “expected relaxation times” as obtained from eq. (2) and (3) for the experiments with $T_D = T_A$ (for
 182 which, consequently, $t_D = t_A/2$) (cf. Berndt et al., 2017).

183 4.4 Determination of the attempt time τ_0

184 Eq. (2) and (3), and therefore the slope of nomograms, strongly depend on the attempt time τ_0 . The
 185 attempt time is determined from the VRM data only using a least-squares optimisation: Either side of
 186 eq. (2) is equal to the blocking volume V_B . Therefore, $\ln(V_B)$ is calculated from T_A and t_A on the one
 187 hand, and from T_D and t_D on the other hand. The difference between the two $\ln(V_B)$ is then minimised
 188 by (iteratively) adjusting τ_0 until the best fit is found. Using only VRM data for the optimisation allows
 189 to test the validity of the predictions of the cooling rate effect (i.e. pTRMs, eq. (3)).

190 4.5 Data correction and rejection criteria

191 A few of the measured demagnetisation curves had to be excluded from the analysis, mostly due to rea-
 192 sons relating to the way the MPMS operates. The MPMS measures magnetic moments by physically
 193 moving the sample through a set of superconducting coils and measuring the change in the induced
 194 current during this process. The arrangement of the coils gives rise to a characteristic curve of induced
 195 current versus sample position with multiple (positive and negative) peaks; a model curve is then fitted
 196 to the measured current curve, from which both the magnetic moment and the exact sample position
 197 is determined. This procedure is intrinsically problematic for measuring magnetic moments close to
 198 zero. In such cases, the amplitude of the induced currents is small and the fitting routine becomes

Table 1. Summary of fitted parameters. ‘CTD’: parameters obtained in a previous study using continuous thermal demagnetisation (Berndt et al., 2017).

Sample		p	τ_0
Magnetoferitin	This study	76 %	8×10^{-8} s
	CTD	54 %	9×10^{-9} s
TC04-12-01	This study	57 %	2×10^{-9} s
	CTD	82 %	1×10^{-13} s

199 error-prone with respect to both moment and positioning – any incorrect fit in the positioning will lead
 200 to an incorrect fit to the magnetic moment. Fortunately, however, this mismatch in positioning tends
 201 to occur in a very consistent way – the magnetic moment tends to be offset by a constant value. Much
 202 of the data where this happened could therefore be corrected by applying a constant offset to “match
 203 up” incorrectly fitted data to the correctly fitted data. The details of this procedure are described in the
 204 supplementary material, where the complete raw data is also presented. Some of the experiments could
 205 not be corrected and were excluded from analyses (also described in the supplementary material).

206 5 RESULTS

207 Fig. 2 and 3 show the raw and smoothed demagnetisation curves $M_{VRM}(t)$ and $M_{pTRM}(t)$, together
 208 with the normalised demagnetisation curves $\hat{M}(t)$. The percentages p of the magnetisation decay that
 209 yielded best fits for the demagnetisation temperatures are given in Table 1, together with the best-fit
 210 values of the atomic attempt time τ_0 and are compared to those obtained by Berndt et al. (2017).
 211 Using these best-fit values, nomograms are plotted in Fig. 4, along with the acquisition values T_A and
 212 t_A and demagnetisation values T_D and t_D (demagnetisation times are multiplied by two to correct for
 213 the zero-field). The magnetoferitin sample shows an excellent fit of the experimental data for VRMs
 214 (constant temperature acquisition) with the Pullaiah nomograms, while the Tiva Canyon sample is
 215 more noisy. Many of the measured Tiva Canyon demagnetisation curves were of low data quality and
 216 had to be excluded from the analysis due to reasons outlined in the supplementary material.

217 The diamonds in the nomograms (Fig. 4) indicate data for the pTRMs, i.e. acquisition through
 218 cooling, and hence indicate whether or not the cooling rate equation (3) is experimentally confirmed.
 219 Again, for the magnetoferitin sample, the points agree very well with the nomograms, indicating
 220 that eq. (3) is appropriate to convert cooling rates to effective acquisition times. For the Tiva Canyon
 221 sample, however, the slope of the pTRM lines (dashed lines in Fig. 4) is consistently shallower than
 222 the nomograms, which indicates that the measured demagnetisation times were shorter than predicted

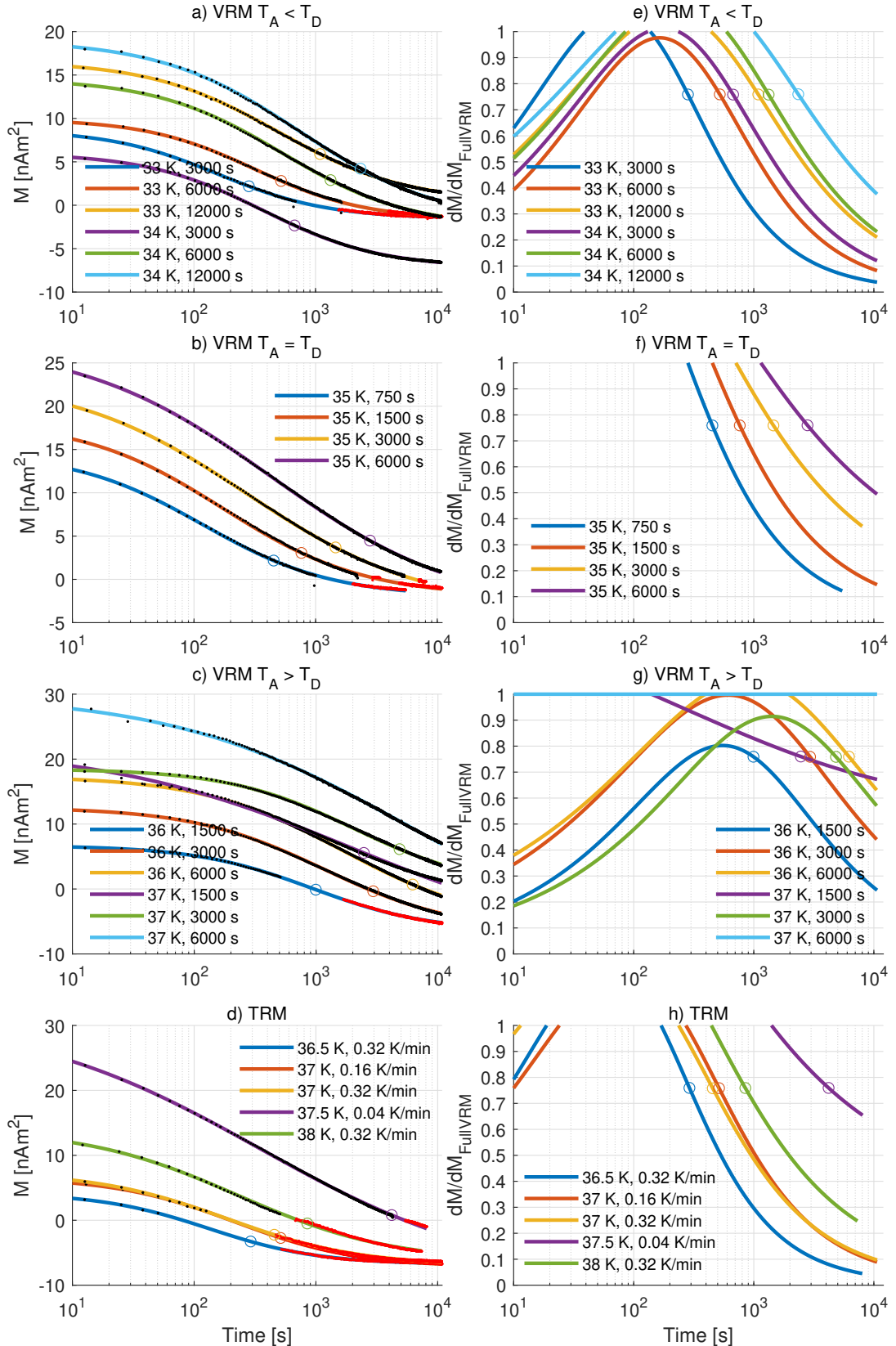


Figure 2. Viscous decay of VRMs (a,b,c) and TRMs (d) for the magnetoferitin sample, all measured at 35 K. (e, f, g, h) Derivatives of viscous decay with respect to the “full VRM” (37 K, 6000 s). Acquisition temperatures and times/cooling rates are indicated in the plots; black dots indicate raw data; solid lines are smoothed data; red dots indicate raw data corrected for positioning errors of MPMS; circles indicate selected relaxation times as described in the text. For colours, refer to the online version of this article.

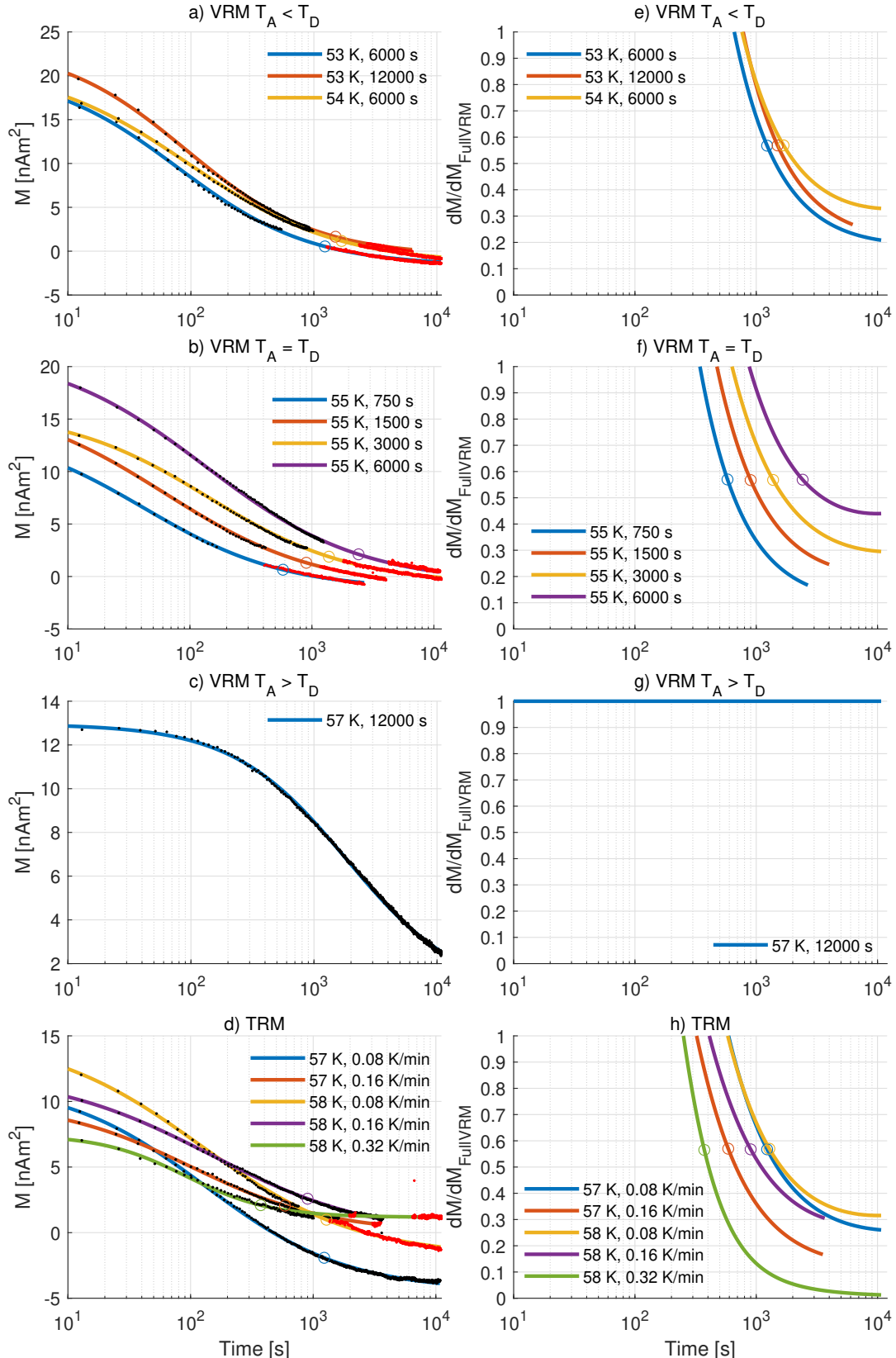


Figure 3. Viscous decay of VRMs (a,b,c) and TRMs (d) for the Tiva Canyon TC04-12-01 sample, all measured at 35 K. Acquisition temperatures and times/cooling rates are indicated in the plots; black dots indicate raw data; solid lines are smoothed data; red dots indicate raw data corrected for positioning errors of MPMS; circles indicate selected relaxation times as described in the text. Derivatives of viscous decay with respect to the “full VRM” (57 K, 12,000 s) are shown in e, f, g, h. For colours, refer to the online version of this article.

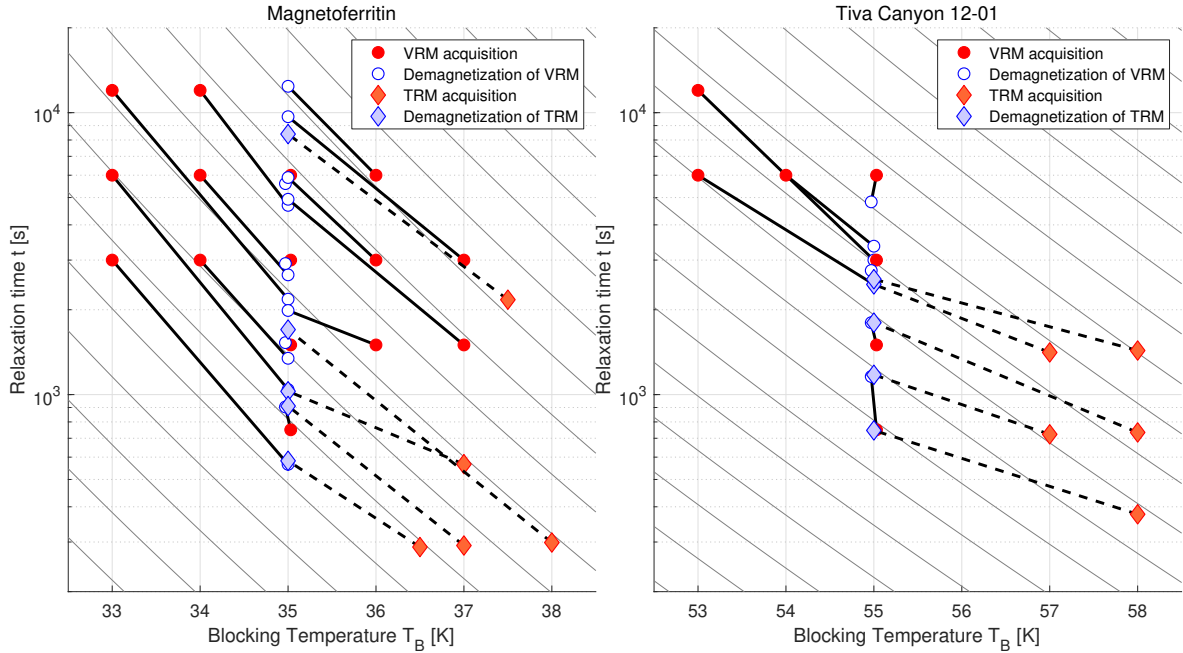


Figure 4. Nomograms of VRMs and TRMs acquired over a given (effective) time t_A and temperature T_A (red) and (viscously) demagnetised at a given demagnetisation temperature T_D after a time t_D (blue). Gray lines indicate nomograms after Pullaiah et al. (1975) for the best-fit values of the attempt time τ_0 . For colours, refer to the online version of this article.

from eq. (2) and (3), or conversely that one would underestimate acquisition times / temperatures when applying the theoretical equations to demagnetisation data from stepwise thermal demagnetisation experiments. This effect is shown more clearly in Fig. 5, which compares acquisition temperatures that would be predicted by applying the equations to the demagnetisation data versus the actual (known) acquisition temperatures. While the predicted T_A agree well with the actual T_A for the magnetoferritin for both VRMs and pTRMs, they are consistently too low (by 1–2 K) for the pTRMs of the Tiva Canyon sample.

6 DISCUSSION

The two studied samples arguably belong to the most ideal (non-interacting SD magnetite) materials that may be encountered in rock magnetism.

The precisely size-controlled nature of the magnetoferritin synthesis might be considered akin to magnetic particles by magnetotactic bacteria, i.e. magnetosomes, that are able to produce similarly well controlled grain sizes and shapes of magnetite and belong to the most ideal natural samples – though these tend to be strongly interacting. The Tiva Canyon sample is a natural sample, which is widely used as a “benchmark” sample for its near ideal non-interacting SD behaviour in studies of fun-

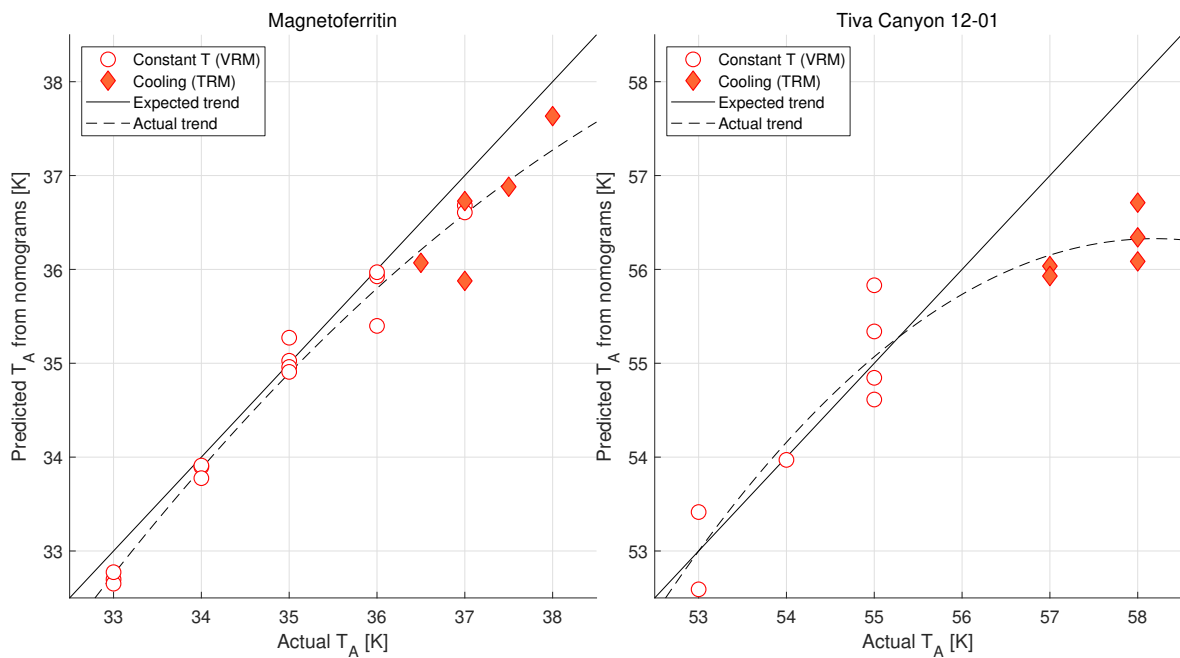


Figure 5. Comparison between the acquisition temperature that would be predicted from the demagnetisation temperatures using Pullaiah et al. (1975) nomograms (Fig. 4), and the actual acquisition temperature that was used in the VRM/TRM acquisition experiments. Dotted line is a polynomial fit. For colours, refer to the online version of this article.

238 fundamental rock magnetism. The two samples here can therefore be considered a “best case” scenario
 239 of cooling rate corrections/blocking temperature estimations of natural materials. As was found in the
 240 experiments, the synthetic magnetoferritin sample followed the theoretical predictions closely – con-
 241 firming that the theoretical framework for cooling rate corrections are sound. The Tiva Canyon Tuff,
 242 however, followed the theoretical predictions only approximately. In particular, the pTRM experiments
 243 showed that the cooling rate equation (3) underestimated the blocking temperature (or conversely the
 244 cooling rate). Possible reasons for this include deviations from ideal non-interacting SD behaviour,
 245 presence of small amounts of secondary magnetic minerals, and surface oxidation of grains. Also, even
 246 though the Verwey transition is suppressed in (low Ti) titanomagnetite, there is still a relatively sharp
 247 increase in M_s around the measured temperature range (Berndt et al., 2015, 2017; Worm & Jackson,
 248 1999) – multi-domain titanomagnetite is known to show anomalous field-cooling, zero-field-cooling
 249 and frequency dependent susceptibility behaviour, possibly due to the suppression of thermally acti-
 250 vated electron hopping (Carter-Stiglitz et al., 2006) that impacts magnetic anisotropy. In our sample,
 251 the grain sizes are, however, much smaller than multi-domain size; nevertheless, this effect may have
 252 impacted the cooling rate behaviour. Additionally, there may be problems related to the experimental
 253 execution such as movement of the sample (or grains in the powdered sample) in the measurement

holder – such problems, however, would only affect individual experiments and likely not lead to a consistent deviation from theory.

In the study of the heating rate effect in continuous thermal demagnetisation experiments, systematic deviations from the theoretical equations were found that had to be corrected for empirically (Berndt et al., 2017). For the cooling rate effect studied here, we did not find the need for any empirical correction. Moreover, the attempt time τ_0 for the Tiva Canyon sample was found in this study to be in the range of commonly cited values for magnetite (2×10^{-9} s) (cf. Berndt et al., 2015), while Berndt et al. (2017) found a very lower of 1×10^{-13} s (Table 1). A possible reason for the difference between the two studies was the magnitude of the applied field (1 mT in Berndt et al. (2017), 50 μ T here). It is therefore possible that fields larger than a few hundred μ T cause deviations from the cooling rate equation. Weak fields similar to the one used here are geologically much more relevant, such that the cooling rate equations can be applied.

Finally, our pTRM acquisition experiments exhibit a strong dependence on cooling rate that highlight shortfalls in applying SD cooling rate theory to palaeointensity data from natural samples: Comparing the pTRM acquisition for the magnetoferitin acquired from 37 K at cooling rates of 0.16 and 0.32 K/min, we find that halving the cooling rate increases the pTRM intensity by $\sim 7\%$. A similar comparison for the Tiva Canyon Tuff pTRMs acquired from 58 K at cooling rates of 0.16 and 0.32 K/min, indicates a pTRM increase of $\sim 43\%$ for a halving of cooling rate. A factor 2 change in the cooling rate is only predicted to change the remanence intensity by a factor of $\sim 1-2\%$ (Halgedahl et al., 1980). This discrepancy is likely related to the often-overlooked fact that cooling rate corrections are blocking temperature dependent (Dodson & McClelland-Brown, 1980): At low T_B the cooling rate effect is enhanced, which might explain the large discrepancies. Combined with the effects of non-linear Newtonian cooling (Yu, 2011), this effect might also produce small degrees of curvature in Arai plots.

Although some studies have illustrated large, but variable cooling rate corrections in igneous materials (e.g. Yu, 2011; Santos & Tauxe, 2019), statistical analyses indicate that most palaeointensity studies from igneous rocks accurately identify a known mean value (e.g. Paterson et al., 2010a, 2014). This suggests that the effect of cooling rates are small and contribute to data scatter, or that the typical data selection processes screen out these effects.

283 7 CONCLUSIONS

284 In conclusion, the experiments show that the cooling rate correction eq. (3) by York (1978a,b) holds
285 and can be applied to non-interacting SD particles. It does, however, also show that even slight devi-

286 autions from this ideal case have a potentially significant effect on cooling rate corrections. This has
 287 important implications for a number of palaeomagnetic applications:

288 (i) A direct application of this result is the estimation of emplacement temperatures of e.g. pyroclas-
 289 tic deposits (Kent et al., 1981; Paterson et al., 2010b) and intrusive rocks / dikes (Hyodo et al., 1993):
 290 These rocks acquire pTRMs upon reheating, the temperature of which can be estimated from unblock-
 291 ing temperatures in stepwise thermal demagnetisation experiments. Our results show that these can be
 292 obtained from nomograms and the equations by York (1978a,b), but that the samples must be carefully
 293 tested for mineralogy (ideally uniform) and domain states (ideally SD).

294 (ii) Our results show that VRM dating, used to estimate deposition times of flood deposits (Sato
 295 et al., 2014), glacial moraines (Crider et al., 2015), landslides (Smith & Verosub, 1994), as well as
 296 archaeological constructions (Heller & Markert, 1973; Borradaile, 1996) from stepwise thermal de-
 297 magnetisation experiments should yield accurate time estimates. The same is true for thermoviscous
 298 problems such as inferring either times or temperatures of reheating associated with burial of rocks
 299 (Kent, 1985; Kent & Miller, 1987). These applications appear to be less critically dependent on the
 300 presence of ideal non-interacting stoichiometric SD grains.

301 (iii) For VRM dating using continuous thermal demagnetisation (Muxworthy et al., 2015; Berndt &
 302 Muxworthy, 2017), our results suggest that, contrary to Berndt et al. (2017), VRM ages obtained from
 303 effective demagnetisation temperatures should be accurate, too, for magnetic fields of the strength of
 304 the geomagnetic field.

305 (iv) Like other studies (Santos & Tauxe, 2019), we found a large variability of the cooling rate effect
 306 on palaeointensities, that is T_B -dependent. This highlights the importance of determining the cooling
 307 rate effect on palaeointensities on a per-sample basis, rather than solely relying on the theoretical
 308 correction.

309 8 APPENDIX

310 ACKNOWLEDGMENTS

311 This study was supported by a Boya Post-doctoral fellowship funded by Peking University and an
 312 Institute for Rock Magnetism (IRM) Visiting Researcher Fellowship to T.A.B.; a National Natural
 313 Science Foundation of China (NSFC) grant (no. 41574063) and a Natural Environmental Research
 314 Council Independent Research Fellowship (NE/P017266/1) to G.A.P.; a NSFC grant (no. 41774076)
 315 to C.C.; and a NSFC grant (no. 41722402) to L.C. The IRM is a US National Multi-user Facility
 316 supported through the Instrumentation and Facilities program of the National Science Foundation,
 317 Earth Sciences Division, and by funding from the University of Minnesota. The manuscript benefited

[!hp]

Table 2. List of symbols and acronyms.

Symbol	Explanation
NRM	Natural remanent magnetisation
(p)TRM	(Partial) Thermoremanent magnetisation
VRM	Viscous remanent magnetisation
Full VRM	A VRM acquired over a very long time such that it is not completely demagnetised in any experiment
SP	Super-paramagnetic
SD	Single-domain
MD	Multi-domain
MPMS	Magnetic Properties Measurement System
CTD	Continuous thermal demagnetisation
STD	Stepwise thermal demagnetisation
FORC	First-order reversal-curves
T_A	Acquisition temperature (blocking temperature in field)
t_A	Acquisition time (relaxation time in field)
T_D	Demagnetisation temperature (blocking temperature in zero-field)
t_D	Demagnetisation time (relaxation time in zero-field)
$T_{A,full}$	Acquisition temperature to impart a ‘Full VRM’ (37 K for the magnetoferitin, 57 K for Tiva Canyon)
$t_{A,full}$	Acquisition time to impart a ‘Full VRM’ (6000 s for the magnetoferitin, 12,000 s for Tiva Canyon)
T_C	Curie temperature
t_{eff}	Effective relaxation time (for continuous cooling or heating at rate r)
τ_0	Atomic attempt time
r_A	Cooling rate of TRM acquisition (in field)
$M_r(T)$	Remanent magnetisation as a function of temperature
$M_r(t)$	Remanent magnetisation as a function of time
$M_s(T)$	Spontaneous magnetisation
$M_{VRM}(t)$	Remanent magnetisation of a VRM measured over time t
$M_{pTRM}(t)$	Remanent magnetisation of a pTRM measured over time t
$M_{VRM} \text{ or } M_{pTRM}(t)$	Either $M_{VRM}(t)$ or $M_{pTRM}(t)$
\hat{M}	Normalised magnetisation defined through the differential of the remanent magnetisation over the differential the full VRM
H_0	Applied magnetic field
$f(V)$	Grain size distribution
$n(V)$	Net proportion of grains of volume V magnetised along the field direction
V_B	Blocking volume
p	Proportion of the initial magnetisation at which the sample is considered demagnetised

³¹⁸ from the efforts of Y. Yu and multiple anonymous reviewers. The experimental data as well as the code³¹⁹ to analyse and plot it are freely available on <https://github.com/thomasberndt>.

320 **References**

- 321 Aharoni, A., 2000. *Introduction to the Theory of Ferromagnetism*, Oxford Univ. Press, Oxford, 2nd
322 edn.
- 323 Berndt, T. A. & Muxworthy, A. R., 2017. Dating Icelandic glacial floods using a new viscous rema-
324 nent magnetization protocol, *Geology*, **45**(4), 339–342.
- 325 Berndt, T. A., Muxworthy, A. R., & Paterson, G. A., 2015. Determining the magnetic attempt time τ_0 ,
326 its temperature dependence, and the grain size distribution from magnetic viscosity measurements,
327 *Journal of Geophysical Research: Solid Earth*, **120**(11), 7322–7336.
- 328 Berndt, T. A., Paterson, G. A., Cao, C., & Muxworthy, A. R., 2017. Experimental test of the heating
329 and cooling rate effect on blocking temperatures, *Geophysical Journal International*, **210**(1), 255–
330 269.
- 331 Biggin, A. J., Badejo, S., Hodgson, E., Muxworthy, A. R., Shaw, J., & Dekkers, M. J., 2013. The
332 effect of cooling rate on the intensity of thermoremanent magnetization (TRM) acquired by assem-
333 blages of pseudo-single domain, multidomain and interacting single-domain grains, *Geophysical
334 Journal International*, **193**(3), 1239–1249.
- 335 Borradaile, G. J., 1996. An 1800-year archeological experiment in remagnetization, *Geophysical
336 Research Letters*, **23**(13), 1585–1588.
- 337 Brown, W. F., 1963. Thermal fluctuations of a single-domain particle, *Journal of Applied Physics*,
338 **34**(1951).
- 339 Cao, C., Tian, L., Liu, Q., Liu, W., Chen, G., & Pan, Y., 2010. Magnetic characterization of nonin-
340 teracting, randomly oriented, nanometer-scale ferrimagnetic particles, *Journal of Geophysical Re-
341 search*, **115**(B7), B07103.
- 342 Cao, C., Wang, X., Cai, Y., Sun, L., Tian, L., Wu, H., He, X., Lei, H., Liu, W., Chen, G., Zhu, R.,
343 & Pan, Y., 2014. Targeted in vivo imaging of microscopic tumors with ferritin-based nanoprobes
344 across biological barriers, *Advanced Materials*, **26**(16), 2566–2571.
- 345 Carter-Stiglitz, B., Moskowitz, B., Solheid, P., Berquó, T. S., Jackson, M., & Kosterov, A., 2006.
346 Low-temperature magnetic behavior of multidomian titanomagnetites: TM0, TM16, and TM35,
347 *Journal of Geophysical Research: Solid Earth*, **111**(12), 1–12.
- 348 Crider, J. G., Globokar, D. M., Burmester, R. F., & Housen, B. A., 2015. Unblocking tempera-
349 tures of viscous remanent magnetism in displaced granitic boulders, Icicle Creek glacial moraines
350 (Washington, USA), *Geophysical Research Letters*, **42**(24), 10,647–10,654.
- 351 Dodson, M. H., 1976. Kinetic processes and thermal history of slowly cooling solids, *Nature*, **259**,
352 551–553.
- 353 Dodson, M. H. & McClelland-Brown, E., 1980. Magnetic blocking temperatures of single-domain

- 354 grains during slow cooling, *Journal of Geophysical Research*, **85**, 2625–2637.
- 355 Dunlop, D. J., 1983. Viscous magnetization of 0.04–100 μm magnetites, *Geophysical Journal International*, **74**, 667–687.
- 356
- 357 Dunlop, D. J. & Özdemir, Ö., 1993. Thermal demagnetization of VRM and pTRM of single domain
358 magnetite: No evidence for anomalously high unblocking temperatures, *Geophysical Research Letters*,
359 **20**(18), 1939–1942.
- 360 Dunlop, D. J., Özdemir, Ö., Clark, D. A., & Schmidt, P. W., 2000. Time-temperature relations for
361 the remagnetization of pyrrhotite (Fe₇S₈) and their use in estimating paleotemperatures, *Earth and*
362 *Planetary Science Letters*, **176**, 107–116.
- 363 Ferk, A., Aulock, F. W. V., Leonhardt, R., Hess, K. U., & Dingwell, D. B., 2010. A cooling rate
364 bias in paleointensity determination from volcanic glass: An experimental demonstration, *Journal*
365 *of Geophysical Research: Solid Earth*, **115**(B8), B08102.
- 366 Fox, J. M. W. & Aitken, M. J., 1980. Cooling-rate dependence of thermoremanent magnetisation,
367 *Nature*, **283**, 462–463.
- 368 Halgedahl, S. L., Day, R., & Fuller, M., 1980. The effect of cooling rate on the intensity of weak-field
369 TRM in single-domain magnetite, *Journal of Geophysical Research*, **85**(80), 3690–3698.
- 370 Heller, F. & Markert, H., 1973. The age of viscous remanent magnetization of Hadrian's Wall (north-
371 ern England), *Geophysical Journal International*, **31**(4), 395–406.
- 372 Hyodo, H., York, D., & Dunlop, D. J., 1993. Tectonothermal history in the Mattawa Area, Ontario,
373 Canada, deduced from paleomagnetism and ⁴⁰Ar/ ³⁹Ar dating of a Grenville Dike, *Journal of*
374 *Geophysical Research: Solid Earth*, **98**(B10), 18001–18010.
- 375 Jackson, M. & Worm, H.-U., 2001. Anomalous unblocking temperatures, viscosity and frequency-
376 dependent susceptibility in the chemically-remagnetized Trenton limestone, *Physics of the Earth*
377 *and Planetary Interiors*, **126**(1), 27–42.
- 378 Jackson, M., Carter-Stiglitz, B., Egli, R., & Solheid, P., 2006. Characterizing the superparamagnetic
379 grain distribution f(V, H_k) by thermal fluctuation tomography, *Journal of Geophysical Research*,
380 **111**(B12), B12S07.
- 381 Kent, D. V., 1985. Thermoviscous remagnetization in some Appalachian limestones, *Geophysical*
382 *Research Letters*, **12**(12), 3–6.
- 383 Kent, D. V. & Miller, J. D., 1987. Redbeds and thermoviscous magnetization theory, *Geophysical*
384 *Research Letters*, **14**(4), 327–330.
- 385 Kent, D. V., Ninkovich, D., Pescatore, T., & Sparks, S. R. J., 1981. Palaeomagnetic determination of
386 emplacement temperature of Vesuvius AD 79 pyroclastic deposits, *Nature*, **290**(5805), 393–396.
- 387 McClelland, E. A. & Druitt, T. H., 1989. Palaeomagnetic estimates of emplacement temperatures of

- 388 pyroclastic deposits on Santorini, Greece, *Bulletin of Volcanology*, **51**(1), 16–27.
- 389 Muxworthy, A. R. & Heslop, D., 2011. A Preisach method for estimating absolute paleofield intensity
390 under the constraint of using only isothermal measurements: 1. Theoretical framework, *Journal of
391 Geophysical Research*, **116**(B4), B04102.
- 392 Muxworthy, A. R., Heslop, D., Paterson, G. A., & Michalk, D., 2011. A Preisach method for esti-
393 mating absolute paleofield intensity under the constraint of using only isothermal measurements: 2.
394 Experimental testing, *Journal of Geophysical Research*, **116**(B4), B04103.
- 395 Muxworthy, A. R., Evans, M. E., Scourfield, S. J., & King, J. G., 2013. Paleointensity results from the
396 late-Archaean Modipe Gabbro of Botswana, *Geochemistry, Geophysics, Geosystems*, **14**(7), 2198–
397 2205.
- 398 Muxworthy, A. R., Williams, J., & Heslop, D., 2015. Testing the use of viscous remanent magneti-
399 sation to date flood events, *Frontiers in Earth Science*, **3**, 1–9.
- 400 Néel, L., 1949. Théorie du traînage magnétique des ferromagnétiques en grains fins avec applications
401 aux terres cuites, *Annales de Géophysique*, **5**, 99–136.
- 402 Paterson, G. A., Heslop, D., & Muxworthy, A. R., 2010a. Deriving confidence in paleointensity
403 estimates, *Geochemistry, Geophysics, Geosystems*, **11**(7), 1–15.
- 404 Paterson, G. A., Roberts, A. P., MacNiocaill, C., Muxworthy, A. R., Gurioli, L., Viramonté, J. G.,
405 Navarro, C., & Weider, S., 2010b. Paleomagnetic determination of emplacement temperatures of
406 pyroclastic deposits: an under-utilized tool, *Bulletin of Volcanology*, **72**(3), 309–330.
- 407 Paterson, G. A., Tauxe, L., Biggin, A. J., Shaar, R., & Jonestrask, L. C., 2014. On improving the
408 selection of Thellier-type paleointensity data, *Geochemistry, Geophysics, Geosystems*, **15**, 1180–
409 1192.
- 410 Pullaiah, G., Irving, E., Buchan, K. L., & Dunlop, D. J., 1975. Magnetization changes caused by
411 burial and uplift, *Earth and Planetary Science Letters*, **28**, 133–143.
- 412 Santos, C. N. & Tauxe, L., 2019. Investigating the Accuracy, Precision, and Cooling Rate Depen-
413 dence of Laboratory-Acquired Thermal Remanences During Paleointensity Experiments, *Geochem-
414 istry, Geophysics, Geosystems*, **20**(1), 383–397.
- 415 Sato, T., Nakamura, N., Goto, K., Kumagai, Y., Nagahama, H., & Minoura, K., 2014. Paleomag-
416 netism reveals the emplacement age of tsunamigenic coral boulders on Ishigaki Island, Japan, *Ge-
417 ology*, **42**(7), 603–606.
- 418 Schlinger, C. M., Veblen, D. R., & Rosenbaum, J. G., 1991. Magnetism and magnetic mineralogy
419 of ash flow tuffs from Yucca Mountain, Nevada, *Journal of Geophysical Research*, **96**(B4), 6035–
420 6052.
- 421 Smith, R. T. & Verosub, K. L., 1994. Thermoviscous Remanent Magnetism of Columbia River Basalt

- 422 Blocks in the Cascade Landslide, *Geophysical Research Letters*, **21**(24), 2661–2664.
- 423 Till, J. L., Jackson, M., Rosenbaum, J. G., & Solheid, P., 2011. Magnetic properties in an ash flow
424 tuff with continuous grain size variation: A natural reference for magnetic particle granulometry,
425 *Geochemistry, Geophysics, Geosystems*, **12**(7), Q07Z26.
- 426 Verwey, E. J. W., 1939. Electronic conduction of magnetite (Fe_3O_4) and its transition point at low
427 temperatures, *Nature*, **144**, 327–328.
- 428 Worm, H.-U. & Jackson, M., 1999. The superparamagnetism of Yucca Mountain Tuff, *Journal of
429 Geophysical Research*, **104**, 25415–25425.
- 430 York, D., 1978a. Magnetic blocking temperature, *Earth and Planetary Science Letters*, **39**, 94–97.
- 431 York, D., 1978b. A formula describing both magnetic and isotopic blocking temperatures, *Earth and
432 Planetary Science Letters*, **39**, 89–93.
- 433 Yu, Y., 2011. Importance of cooling rate dependence of thermoremanence in paleointensity determi-
434 nation, *Journal of Geophysical Research*, **116**(B9), B09101.